Int. J. Electrochem. Sci., 13 **(2018)** 5460 – 5473, doi: 10.20964/2018.06.76

International Journal of
ELECTROCHEMICAL
SCIENCE
www.electrochemsci.org

Prediction of Surface Roughness in Abrasive Assisted Electrochemical Jet Machining of Micro-Channels

Kai Zhao[1,*], *Changshui Gao* [1,*], *Zhuang Liu*[1,**], *Chao Guo*[2]

[1] College of Mechanical and Electrical Engineering, Nanjing University of Aeronautics and Astronautics, Nanjing 210016, China.
[2] Jiangsu Key Laboratory of Precision and Micro-Manufacturing Technology, Nanjing 210016, China.
[*]These authors contributed equally to this work and should be considered co-first authors.
[**]E-mail: liuzhuang@nuaa.edu.cn

Received: 10 February 2018 / *Accepted:* 12 April 2018 / *Published:* 10 May 2018

Abrasive assisted electrochemical jet machining (AECJM) is capable of fabricating micro-channels effectively at metal surface through erosion, corrosion and synergistic effect simultaneously. The complex mechanism of material removal results in significant difficulties to describe surface topography and predict surface roughness of a micro-channel produced by AECJM. This paper established a mathematical model for accurately predicting areal roughness (S_a) of micro-channels due to AECJM of SS304. Six main factors, i.e. working voltage (U), concentration of abrasive (C_a), electrolyte concentration (C_s), jet pressure (P), jet scan speed (V) and passes (N) have been considered in establishing the model. An orthogonal experiment was conducted to investigate the effects of the six main factors and two-factor interactions on S_a through regression analysis. The results reveal that the main factors influence the mean S_a with an importance of order as V–N–C_a–C_s–P–U. Working voltage, jet pressure and six two-factor interactions exhibit unmarked influences on the S_a, and have been eliminated from the model for purpose of simplification. The validation showed that the prediction agrees with experimental data with a maximum error of 12.2% and an average error of 3.5%.

Keywords: abrasive assisted electrochemical jet machining; electrochemical jet machining; micro-channel; surface roughness

1. INTRODUCTION

Micro-channels have been increasingly used in micro-electromechanical systems (MEMS) and micro fluidics systems [1-4]. Jet machining processes, e.g. abrasive water jet machining (AWJM) and electrochemical jet machining (ECJM), have shown notable capability of fabricating micro-channels in a variety of materials with absence of burrs, heat affect zone and pre-formed tools, and good surface integrity [5-6].

AWJM can machine micro-channels through eroding material with a high speed jet mixed with abrasives and water. Recently, Haghbin presented a high-pressure (up to 250 MPa) abrasive slurry micro-machining system and through which they made micro-channels in material Al6061-T6 with a ø254 μm jet mixed with 25 μm abrasives [7]. Khahipour investigated formation of channels in glass machined by AWJM, and they found that a jet pressure of 250 MPa and an impact angle of 75 degree achieved an optimized depth and surface quality [8]. In the meantime, many literatures also reported AWJM of micro-channels with low-pressures (less than 10 MPa). For example, Kowsari studied influences of process conditions on machining roughness of micro-channels result from AWJM at materials of glass, PMMA and ceramics, with a jet pressure less than 6 MPa [9]. Literature [10] reported an investigation of AWJM of micro-channels with low-pressure in quartz crystals, and found that surface roughness and material removal rate increase with jet pressure, particle size, impact angle and concentration of abrasive, but decrease with the nozzle scan speed.

ECJM process can remove metals and form micro-channels at target surface through anodic dissolution [11]. Recently, Liu studied ECJM of dimples and channels at TB6 titanium alloy [2]. Speidel found that using solution of sodium chloride (NaCl) could achieve a double material removal rate than using solution of sodium nitrate ($NaNO_3$) during ECJM of titanium alloy [12]. Guo investigated feasibility of machining mesoscale channels in stainless steel using a scanning micro electrochemical flow cell [13]. Hackert-Oschätzchen studied ECJM of step holes, grooves and pocket in tungsten carbide alloys [14].

Abrasive assisted electrochemical jet machining (AECJM) is a hybrid process coupling AWJM and ECJM methods concurrently. The AECJM can effectively machine micro-channels in metals through erosion, corrosion and synergistic effect simultaneously [15]. Liu employed a AECJM apparatus with low pressure jet to machine micro-channels at tungsten carbide, and they found that the passivation layer can be removed efficiently by particles impingement [16]. In another study, he compared the machining performance of AWJM, ECJM and AECJM, and revealed that the material removal rate of AECJM is markedly greater than AWJM and ECJM alone [17].

The surface roughness of micro-channel is a critical characteristic because it can significantly affect the fluidic performance [18-19]. Therefore, it is highly necessary to accurately predict surface roughness before AECJM operation. At present, the roughness of machining surface can be predicted by theoretical, empirical or semi-empirical approaches. Examples of theoretical method include Jafar [19] and Schwartzentruber [20], who established theoretical models to predict roughness machined by AWJM on a basis of material removal mechanisms. Empirical or semi-empirical models can be used for some cases that are difficult to describe the surface topography. For instance, Kouravand developed an empirical model to forecast surface roughness of milled micro-channels through studying relationship between cutting condition and roughness [21]. Patil built up a semi-empirical model of surface roughness in wire electro-discharge machining of ceramic particle reinforced Al matrix composites [22].

For AECJM of micro channel, describing the formation of surface topography is great challenging because the synergy of erosion and corrosion remains unpredictable. Therefore, this paper established a predictive model for areal roughness (S_a) of micro-channels result from AECJM. The model was based on a quadratic polynomial integrating six main factors (working voltage, electrolyte

concentration, abrasive dose, jet pressure, jet scan speed and jet scan passes) and two-factor interactions. The effects of the main factors and two-factor interactions on S_a were studied through an orthogonal experiment and regression analysis. The model was simplified by eliminating some factors which affect result unremarkably. Finally, the model was verified by experimental data.

2. MODELLING METHOD AND EXPERIMENTAL SETUP

2.1 Modelling of channel roughness

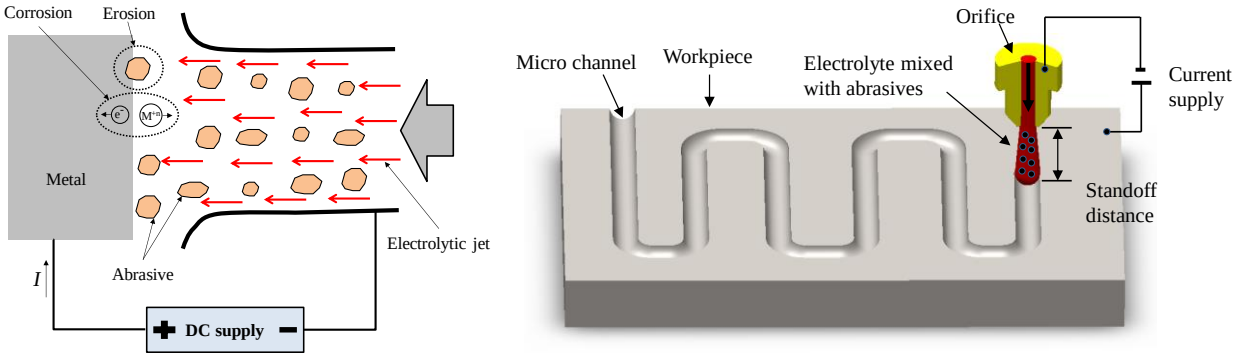

(a) Material removal mechanism (b) AECJM of a micro-channel

Figure 1. Schematic of AECJM process

The AECJM can remove metals through corrosion due to electrochemical reaction and erosion due to abrasives impingement concurrently, as shown in Figure 1(a). Therefore, the material removal of AECJM (M) can be expressed as a sum of mass loss of corrosion (M_1) and erosion (M_2), i.e. $M=M_1+M_2$. According to electrochemical theory, the mass loss rate of anodic dissolution depends on corrosive current (I), electrochemical equivalent (ω), current efficiency (η) and corrosive time (t), i.e. $M_1=\eta\omega It$. From erosion point of view, the mass loss rate due to abrasives impingement (M_2) is relevant to a set of factors such as density, size and velocity of abrasive, and elasticity modulus of abrasive and target material etc. Generally, in case of an AECJM machining with impact angle of 90 degrees, the total mass loss rate can be expressed as:

$$M = \eta\omega It + \varphi K\left(\frac{1-\nu_1^2}{E_1}+\frac{1-\nu_2^2}{E_2}\right)\rho_1(\delta R)^2 V_p{}^2 \qquad (1)$$

Where φ is a constant, K is the total number of impacting abrasives, E_1 and ν_1 are elasticity modulus and Poisson ratio of abrasive, E_2 and ν_2 are elasticity modulus and Poisson ratio of target material, ρ_1 is abrasive's density, δ is roundness factor of abrasives, R is abrasive's radius, and V_p is abrasive's impact velocity.

Figure 1(b) shows the principle of fabricating a micro-channel through AECJM process. Obviously, as demonstrated in Eq.1, a number of factors will influence the process and consequently the surface topography during the AECJM machining. From erosion point of view, the abrasives impingement will create permanent craters on material surface and excess flakes that are easy to separate from the mother material by consecutive abrasives impact [23]. Shape, size, density and

concentration of abrasive, and impacting velocity can notably influence machining result. From corrosion point of view, type and concentration of electrolyte, applied working voltage and inter-electrodes gap distance will significantly influence the anodic dissolution and surface topography [24].

Among the above-mentioned factors, some are easy to be regulated during process, e.g. jet pressure, working voltage, jet scan speed and so on; others are not. From the production point of view, six main factors that are convenient to be controlled have been considered in establishing the empirical model for predicting S_a. They are:

- DC working voltage U (V),
- jet pressure P (MPa),
- concentration of abrasive C_a (wt%),
- electrolyte concentration C_s (wt%),
- jet scan speed V (mm/s), and
- scan passes N.

The unchanged machining conditions are standoff distance of 2 mm, angular abrasives of Al_2O_3 with 1200 mesh size, impinging angle of 90 degrees, electrolyte of $NaNO_3$, jet diameter of 300 μm and target material of SS304. The standoff distance and abrasive size are fixed as 2 mm and 1200 mesh due to a consideration of maintaining stable machining and maximizing material removal rate under present experimental setup. Practically, a gap distance less than 2 mm may result in a nozzle wear due to return flow of the jet involving high speed particles. A gap distance greater than 2 mm will reduce the potential drop between nozzle and target, and consequently drop down anodic dissolution rate.

Areal roughness S_a, representing the arithmetical mean of the height deviations in the surface measured, is selected to evaluate the machining surface roughness in this study. Generally, an empirical prediction can be expressed as an additive model supposed to have effects of main factors (main effects), two-factor interactions and higher-order interactions [25]. The effect hierarchy indicates that main effects are more important than two-factor interactions, while two-factor interactions are more important than higher-order interactions. For purpose of simplification, this paper eliminated higher-order interactions. Thus the S_a can be described as:

$$S_a = a_0 + \sum_{i=1}^{n} a_i x_i + \sum_{i \neq j}^{n} a_{ij} x_i x_j \qquad (2)$$

where the first term of right side (a_0) is a constant coefficient relating to unchanged process conditions, the second term ($\sum_{i=1}^{n} a_i x_i$) is a sum of influences of main effects (x_i is the value of main factor and a_i is the coefficient), the third term ($\sum_{i<j}^{n} a_{ij} x_i x_j$) represents a sum of two-factor interaction ($x_i y_j$ is a product of two factors and a_{ij} is the coefficient), and n represents total number of main factors.

In case of 6 main factors, as studied in this paper, the Eq.2 will become a lengthy formula having one constant term, six linear terms (main effects) and fifteen quadratic terms (two-factor interactions). However, there are probabilities that the impact of some main effects and two-factor interactions on the result are very low. Therefore, it is highly necessary to reduce the model by identifying these factors and interactions through experiments and putting their effect into the constant term (a_0) of Eq.2.

2.2 Experimental apparatus and result inspection

Figure 2 shows schematic of the experimental apparatus used in this study. The apparatus consists of a fluid supply, a metering pump, a motion control system and a DC power. The fluid supply is equipped with a fluid tank, containing mixed electrolyte and abrasives, and a stirring motor. The stirred fluid is pressurized by the metering pump and formed an approximately ø300 μm jet through a stationary sapphire orifice. The DC power can provide a voltage up to 200 volts between specimen and metallic nozzle. A slide unit was used to move specimen in two-dimensional direction at a velocity between 0.02 and 5 mm/s. The operating fluid was prepared and mixed in the tank with angular Al_2O_3 particles (mesh size of 1200) and $NaNO_3$ electrolyte. Stainless steel 304 plates, prepared as 50 mm in length, 25 mm in width and 3 mm in thickness, were used as the target material.

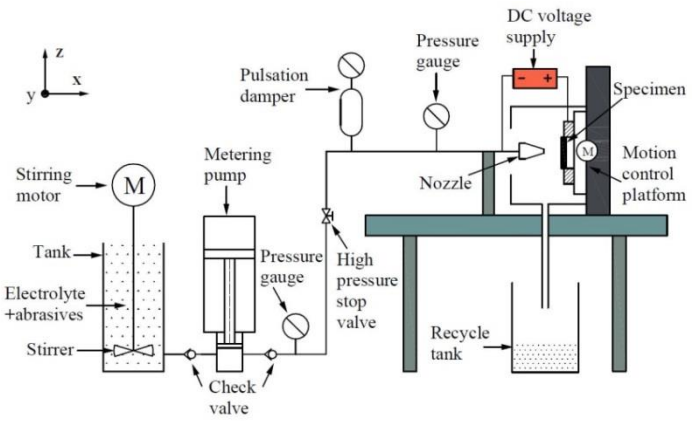

Figure 2. Schematic of experimental apparatus.

Micro-channels have been machined by scanning the specimens below the stationary jet at a speed over a 5 mm length for several consecutive passes. Figure 3 demonstrates a SEM image of a typical micro-channel machined by AECJM with standoff distance of 2 mm, working voltage of 120 V, jet pressure of 3.0 MPa, 1.0 wt% abrasives, 15 wt% $NaNO_3$ electrolyte, jet scan speed of 0.04 mm/s and scan passes of 6. The channel has a width (*W*) of approximate 500 μm, a depth (*H*) of approximate 254 μm and an aspect ratio of 0.5 (*H/W*).

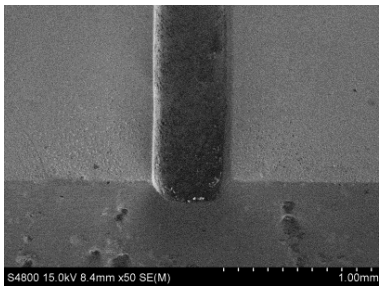

Figure 3. SEM image of a channel machined in SS304

Figure 4 illustrates the schematic of measuring S_a for a micro-channel. For each machined channel, a three dimensional area of 1 mm by 1 mm was inspected in the middle using an optical microscope (Olympus DSX510), with a step size of 4 μm along two planar scanning directions. Afterwards, an areal roughness (S_a) is obtained based on the measured 3D topography with a sampling area of 100×600 μm at bottom of the machined channel.

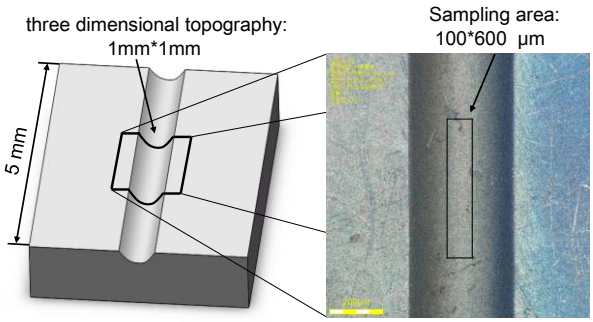

Figure 4. Schematic of measuring S_a for a machined micro-channel

2.3 Design of experiments

Table 1. Experimental factors and levels.

Level	***U*** (V)	C_s (wt%)	C_a (wt%)	***P*** (MPa)	***V*** (mm/s)	***N***
1	80	5	0.5	2	0.04	2
2	100	10	0.75	2.5	0.06	4
3	120	15	1.0	3	0.08	6

The goal of the experiments is to investigate influences of the main factors and their interactions on S_a of the channel. Those factors having minor influences on surface roughness will be identified and integrated into constant term in Eq.1. Table 1 presents the main factors and levels used in the investigation, and a $L_{18}(3^6)$ orthogonal experiment was designed accordingly. Table 2 lists the unchanged conditions during experiment.

Table 2. Constant experimental conditions.

Jet diameter (μm)	Impact angle (°)	Standoff distance (mm)	Abrasive type	Electrolyte composition	Target material
300	90	2.0	Al_2O_3	$NaNO_3$	SS 304

3. RESULTS AND DISCUSSION

3.1 Experimental results

Table 3 lists the experimental design and inspected results (width *W*, depth *H* and roughness S_a) of machined micro-channels according to factors and levels of Table 1. Each experiment was conducted three times, and the values of *W*, *H* and S_a were calculated by mathematically averaging three inspected results. In overall, the eighteen experiments achieved a set of channels having various widths from 340 to 454 μm, depths from 7 to 149 μm, and roughness S_a from 0.33 to 1.07 μm.

Table 3 Experimental design and inspected results

Exp. #	U (V)	C_s (wt%)	C_a (wt%)	P (MPa)	V (mm/s)	N	W (μm)	H (μm)	S_a (μm)
1	120	5	1.0	2.0	0.06	6	418	34	0.70
2	80	5	1.0	3.0	0.08	4	454	22	0.59
3	80	5	0.5	2.0	0.04	2	340	7	0.99
4	100	5	0.5	2.5	0.08	6	396	20	0.77
5	100	5	0.75	3.0	0.06	2	410	15	0.63
6	120	5	0.75	2.5	0.04	4	444	47	0.94
7	120	10	0.5	2.0	0.08	4	370	43	0.70
8	80	10	0.5	3.0	0.06	6	412	63	0.84
9	100	10	0.75	2.0	0.04	6	412	96	1.06
10	80	10	0.75	2.5	0.08	2	427	18	0.33
11	100	10	1.0	2.5	0.06	4	385	47	0.77
12	120	10	1.0	3.0	0.04	2	418	53	0.76
13	120	15	0.5	2.5	0.06	2	406	49	0.66
14	100	15	0.5	3.0	0.04	4	447	122	0.99
15	120	15	0.75	3.0	0.08	6	450	114	0.92
16	80	15	0.75	2.0	0.06	4	400	57	0.71
17	100	15	1.0	2.0	0.08	2	394	33	0.46
18	80	15	1.0	2.5	0.04	6	465	149	1.07

3.2 Investigation of main effects on channel depth and width

Figure 5 demonstrates plot of main effects on depth and width of machined channels in Table 3. It can be seen in Figure 5(a) that influences of electrolyte concentration, scanning speed and passes on machined depth were more significant than that of other factors. Scanning speed (*V*) and passes (*N*) of jet determined total time of material removal involving both corrosion and erosion, while electrolyte concentration (C_s) only related with corrosion. This reveals that mass loss due to corrosion was markedly greater than that due to erosion in AECJM of stainless steel. This agrees with the conclusion of literature [17] where the authors found that anodic dissolution dominates the material removal in AECJM process. For instance, the channel depth (*H*) increased 120% when C_s increased from 5 to 10 wt%, while increasing concentration of abrasive (C_a) from 0.5 to 1 wt% only resulted in a 20% increase of *H*. According to Faraday's law, the velocity of anodic dissolution v_n can be obtained by:

$$\overrightarrow{v_n} = \eta \cdot \frac{\omega}{\rho} \cdot \kappa \cdot \overrightarrow{E_n} \quad (3)$$

where ρ is the density of the workpiece material, κ is the electrolyte electrical conductivity and E_n is the electric field intensity at anode [26-27]. Obviously, the anodic dissolution increases with κ which can be significantly affected by factor C_s. For example, the literature [14] found that electrical conductivity of electrolyte approximately increased 50% when the mass fraction of salts was doubled.

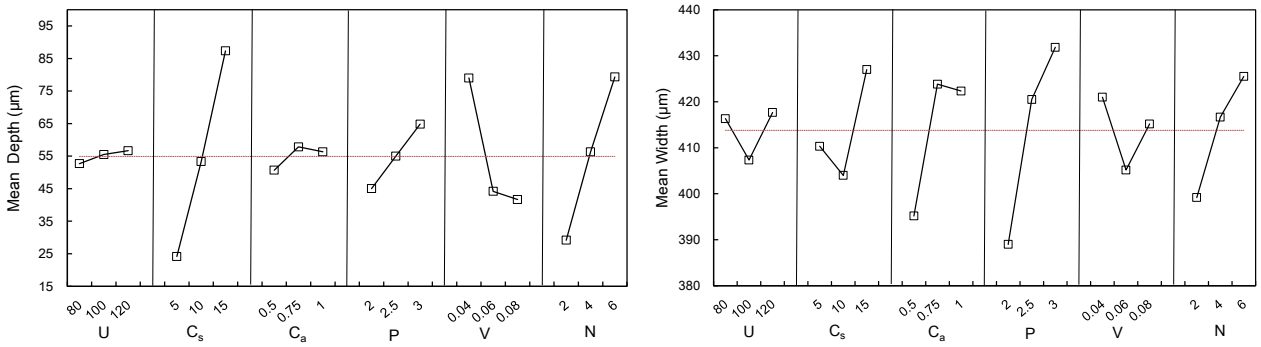

(a) main effects on depth (b) main effects on width

Figure 5. Plot of main effects on depth and width of machined channels

Figure 5(b) shows that the jet pressure (*P*) is the most notable factor affecting the width (*W*) of machined channels. This can be explained by secondary removal caused by rebound flow on sidewall of machining channels. Some literatures verified that part of the jet will immediately rebound after impinging workpiece and form a secondary viscous flow on sidewall of machining area [8][28]. This return flow can erode the sidewall due to shear effect of abrasives. Obviously, increasing jet pressure will result in higher kinetic energy of particles involved in the return jet, and subsequently lead to broader channel. This is also verified by Pang who found that water pressure is the major parameter affecting the channel width in AWJ of microchannel in glass [29].

3.3 Investigation of main effects and two-factor interactions on surface roughness

Figure 6 illustrates the plot of main effects on S_a of the machined channels. Each data point in Figure 6 represents a mean S_a of the experiments associated with a level of a main factor. For a specific factor, the main effects plot indicates the averaged change of response caused by a change of that factor. As can be seen in the figure, the six main factors influence the S_a with an importance of order as *V–N–*C_a*–*C_s*–P–U*. The jet scan speed (*V*) and scan passes (*N*) have the most significant impact on the mean S_a. For example, the mean S_a decreases 27% and 35% when jet scan speed increases from 0.04 to 0.08 mm/s with a step size of 0.02 mm/s. Similarly, increasing jet scan passes from 2 to 6 with step size of 2 results in an increase of 22% and 40% of mean S_a. This result probably relates with the machining mechanism of AECJM, in which the anodic dissolution dominates the material removal, while the particles impingement can hardly erode stainless steel but notably influence the redox reaction at present condition [30]. In general, decreasing jet scan speed *V* or increasing scan passes *N* will result in an increase of total amount of metal corroded, and lead to a greater non-uniformity of

components dissolution and subsequently more micro pits at machining surface. These micro pits can be removed by consecutive abrasives impact; nevertheless, the generation of the micro pits may faster than removal of that.

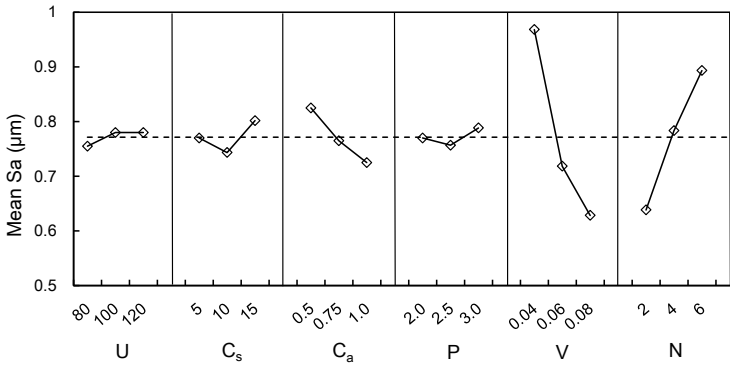

Figure 6. Plot of main effects on S_a.

Figure 6 also shows that the working voltage (U) and jet pressure (P) have relatively low influences on the surface roughness. For example, the mean S_a increases only 4% during the increase of working voltage from 80 to 120 V. Similarly, the mean S_a changes approximate only 4% as jet pressure varied from 2 to 3 MPa. This result is consistent with the findings of literature [30], in which the surface roughness P_a of channel centerline is almost independent with working voltage in AECJM of micro channels at material SS304. The jet pressure also shows insignificant influence on mean S_a, probably because that the jet pressure ranging between 2 and 3 MPa cannot notably disturb the material removal process and the machining topography. This agrees again with the findings of literature [30], in which the material removal rate and roughness P_a changed a little during the increases of jet pressure from 2 to 3 MPa in a single factor experiment of AECJM. Therefore, it is highly necessary to remove factors U and P from the linear terms ($\sum_{i=1}^{n} a_i x_i$) of Eq. 2 for the purpose of simplifying the empirical model.

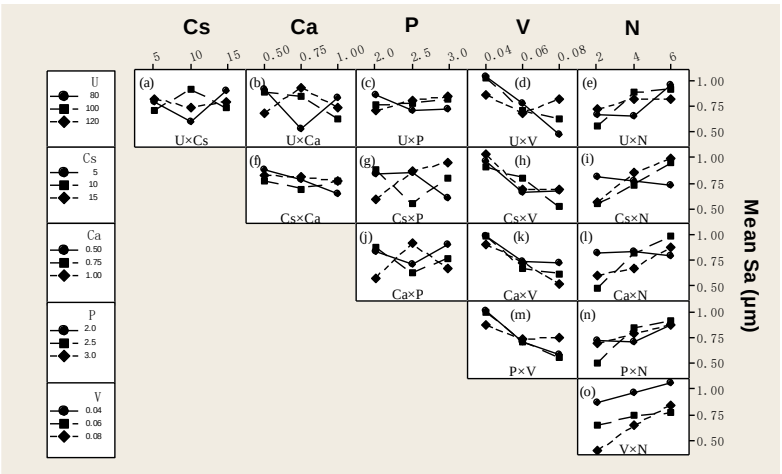

Figure 7. Plot of two-factor interactions on S_a.

Figure 7, exported from Minitab system, illustrates effects of the fifteen two-factor interaction on S_a. Each data point in Figure 6 represents a mean S_a of experiments associated with each level of a factor with the level of a second factor held constant. This plot is useful for judging the presence of interaction when the response at a factor level depends upon the level of other factor. Parallel lines in an interactions plot indicate no interaction. The greater the departure of the lines from the parallel state, the higher the degree of interaction. As can been seen in Figure 7, compared to other sub-graphs, the sub-graphs of (c), (f), (h), (k), (m) and (o) exhibit relative lower interaction on the result. Thus, for purpose of simplification, the two-factor interactions of *U*×*P*, *Cs*×*Ca*, *Cs*×*V*, *Ca*×*V*, *P*×*V* and *V*×*N* are removed from quadratic terms ($\sum_{i\neq j}^{n} a_{ij} x_i x_j$) of Eq. 1, and the number of that terms can be reduced from fifteen to nine.

3.3 Solution of the predictive model

As previously analyzed, the numbers of linear terms and quadratic terms of Eq.2 can be cut to four and nine, respectively. The effect of those removed will be integrated into the constant term of the model. Thus, the model will become:

$$S_a = a_0 + a_1 C_s + a_2 C_a + a_3 V + a_4 N + a_5 U C_s + a_6 U C_a + a_7 U V + a_8 U N + a_9 C_s P + a_{10} C_s N + a_{11} C_a P + a_{12} C_a N + a_{13} P N \quad (4)$$

As can be seen in Eq.4, there are fourteen coefficients (a_0,…,a_{13}) need to be determined. These coefficients can be calculated using regression analysis according to the experimental data in Table 3. Therefore, the final expression of the empirical model can be described as:

$$S_a = 1.16 - 0.0858 C_s + 2.68 C_a - 20.3 V - 0.077 N + 0.000659 U C_s - 0.0169 U C_a + 0.0885 U V + 0.00073 U N - 0.004 C_s P + 0.00625 C_s N - 0.219 C_a P - 0.128 C_a N + 0.0414 P N \quad (5)$$

3.4 Model validation

Table 4. Model validation of experiments in Table 3.

Exp. #	Inspected S_a (μm)	Predicted S_a (μm)	Error (%)	Exp. #	Inspected S_a (μm)	Predicted S_a (μm)	Error (%)
1	0.70	0.70	0.0	10	0.33	0.36	-8.3
2	0.59	0.58	1.1	11	0.77	0.75	2.3
3	0.99	0.93	6.0	12	0.76	0.72	5.7
4	0.77	0.72	7.5	13	0.66	0.67	-1.3
5	0.63	0.67	-6.6	14	0.99	0.99	0.0
6	0.94	0.97	-2.6	15	0.92	0.90	2.6
7	0.70	0.71	-1.8	16	0.71	0.67	6.6
8	0.84	0.88	-4.1	17	0.46	0.47	-1.4
9	1.06	1.11	-4.4	18	1.07	1.07	0.0

Table 4 lists a comparison of roughness S_a between experimental results and prediction according to Table 3. The empirical model agreed with the eighteen experimental data, with a maximum error of 8.3% and an average error of 3.5%.

Table 5. Model validation of additional eight experiments.

Exp. #	U (V)	C_s (wt%)	C_a (wt%)	P (MPa)	V (mm/s)	N	Inspected S_a (μm)	Predicted S_a (μm)	Error (%)
19	120	15	0.5	2.5	0.08	2	0.47	0.48	-2.1
20	110	15	0.7	2.5	0.08	5	0.73	0.71	2.8
21	95	10	0.45	2.5	0.06	4	0.72	0.76	-5.3
22	100	15	0.40	3	0.06	4	0.77	0.78	-1.3
23	125	15	0.65	3	0.06	4	0.89	0.91	-2.2
24	115	15	0.50	3	0.08	6	0.99	1.03	-3.9
25	80	15	0.8	2.5	0.04	6	1.07	1.07	0.0
26	80	10	1.0	2.5	0.08	2	0.43	0.49	-12.2%

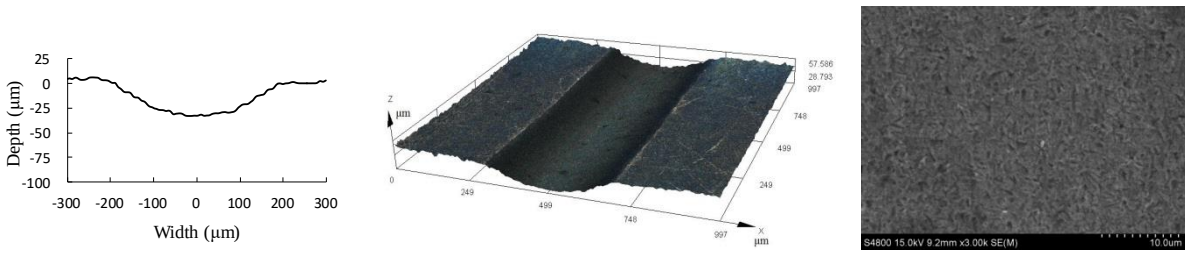

(a) Cross-sectional profile (b) 3D profile (c) SEM image of channel bottom

Figure 8. Measured characteristics of the channel due to experiment #19 (U=120 V, C_s=15 wt%, C_a=0.5 wt%, P=2.5 MPa, V=0.08 mm/s, N=2, predicted S_a=0.48 μm, and measured S_a=0.47 μm, W=393 μm and H=33 μm)

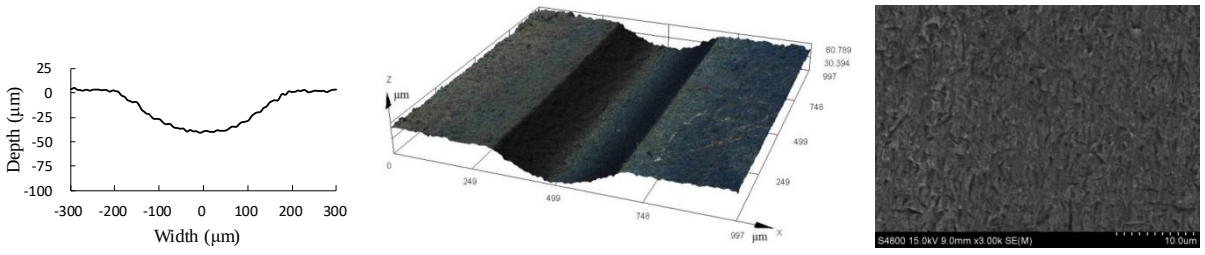

(a) Cross-sectional profile (b) 3D profile (c) SEM image of channel bottom

Figure 9. Measured characteristics of the channel due to experiment #21 (U=95 V, C_s=10 wt%, C_a=0.45 wt%, P=2.5 MPa, V=0.06 mm/s, N=4, predicted S_a=0.76 μm, and measured S_a=0.72 μm, W=363 μm and H=39 μm)

Eight experiments (from #19 to #26) were performed to verify the model additionally, as shown in Table 5. The values of six factors were selected on purpose to make prediction of S_a ranges between 0.48 to 1.07 μm. Similar to the results of Table 4, the model agreed well with the experimental data with a maximum error of 12.2% and an average error of 3.7%. Figures 8, 9 and 10

illustrate measured profiles and surface topographies of three micro-channels machined for experiments of #19, #21, #23 in Table 5. Figure 11 summaries the overall tween-six verification of the model and shows an average predicted error of 3.5%.

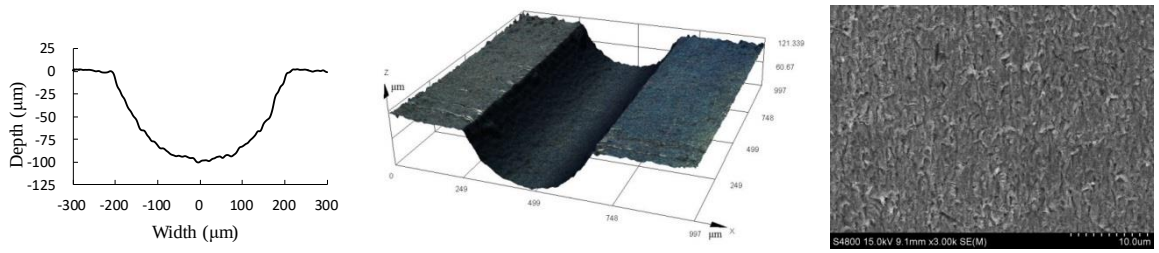

(a) Cross-sectional profile (b) 3D profile (c) SEM image of channel bottom

Figure 10. Measured characteristics of the channel due to experiment #23 (U=125 V, C_s=15 wt%, C_a=0.65 wt%, P=3.0 MPa, V=0.06 mm/s, N=4, predicted S_a=0.91 μm and measured S_a=0.89 μm, W=421 μm and H=99 μm)

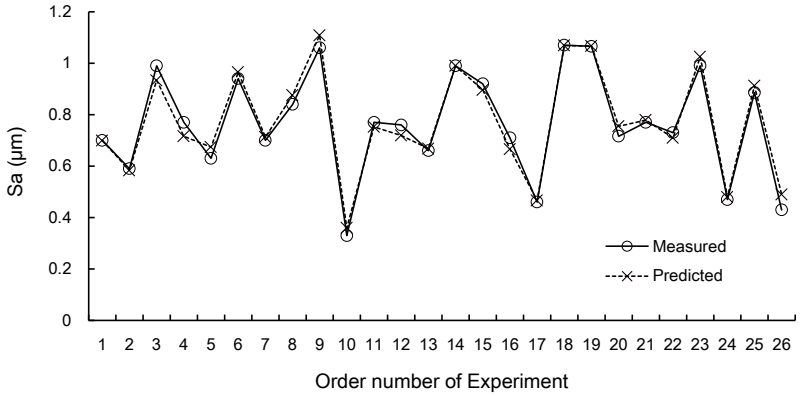

Figure 11. Summary of the verification for the model

According to Figure 6, the probable minimum S_a may be obtained by machining factors of U=80V, C_s=10%, C_a=1%, P=2.5 MPa, V=0.08 mm/s and N=2. For this set of factors, the correspondent machining result has a S_a of 0.43 μm and the predictive model has a output of S_a=0.49 μm (a predicted error of 12.2%). From another hand, the experiment #10 (U=80, C_s=10%, C_a=0.75%, P=2.5 MPa, V=0.08 mm/s and N=2) in Table 5 obtained a prediction of 0.36 μm and an experimental result of 0.33 μm, which are smaller than previous case. This proofed that the main effects plot (Figure 6) is not sufficient to determine process factors for a minimum S_a, although those main effects are more important than two-factor interactions. Thus, in the scope of process conditions presented in this paper, the factors of U=80, C_s=10%, C_a=0.75%, P=2.5 MPa, V=0.08 mm/s and N=2 can achieve a relatively low S_a for AECJM of a micro-channel.

4. CONCLUSIONS

This paper established a model for predicting areal roughness S_a of the micro-channels result from AECJM. The model was based on a quadratic polynomial containing six main factors, i.e.

working voltage (U), electrolyte concentration (C_s), concentration of abrasive (C_a), jet pressure (P), jet scan speed (V) and scan passes (N), and two-factor interactions. The orthogonal experiment reveals that the six main factors influence the mean S_a with an importance of order as V–N–C_a–C_s–P–U. The S_a markedly decreases with V and increases with N, because the anodic dissolution dominates the material removal and a greater amount of metal corroded may result in greater non-uniformity of components dissolution, and subsequently more micro pits at machining surface. The U and P show a relative low influences on mean S_a, which is consistent with the findings of literature [30]. Moreover, six two-factor interactions, i.e. $U\times P$, $C_s\times C_a$, $C_s\times V$, $C_a\times V$, $P\times V$ and $V\times N$, also exhibit insignificant influences on mean S_a. Therefore, these six interactions and two main factors (U and P), have been eliminated from the model for purpose of simplification. The validation shows that the empirical model agreed with twenty-six experimental data with a maximum error of 12.2% and an average error of 3.5%.

ACKNOWLEDGEMENTS

The authors acknowledge the support of National Natural Science Foundation of China (Grant no. 51675273) and Natural Science Foundation of Jiangsu Province (Grant no. BK2015020754). This work was also supported by Foundation of Graduate Innovation Center in NUAA (Grant no. kfjj20170519). The authors also acknowledge Changzhou Institute of Technology for using inspection apparatus.

References

1. T. Bandara, N.T. Nguyen and G. Rosengarten, *Chem. Eng. Sci.*, 126 (2015) 283.
2. W. Liu, S. Ao, Y. Li, Z. Liu, Z. Wang, Z. Luo, Z. Wang and R. Song, *Int. J. Adv. Manuf. Technol*., 90 (2017) 2397.
3. J.D.A. Ziki, T.F. Didar and R. Wüthrich, *Int. J. Mach. Tools Manuf*., 57 (2012) 66.
4. H. Lee, L. Xu, D. Koh, N. Nyayapathi and K.W. Oh, *Sensors*, 14 (2014) 17008.
5. C. Kang and H. Liu, *Materials*, 6 (2013) 3514.
6. J. Meng, Q. Wei and Y. Ma, *Math. Comput. Appl*., 21 (2016) 2.
7. N. Haghbin, F. Ahmadzadeh, J.K. Spelt and M.Papini, *Int. J. Adv. Manuf. Technol*., 84 (2016) 1031.
8. K. Dadkhahipour, T. Nguyen and J. Wang, *Wear*, 292-293 (2012) 1.
9. K. Kowsari, J. Schwartzentruber, J.K. Spelt and M. Papini, *Precis. Eng*., 49 (2017) 332.
10. H. Qi, J. Fan and J.Wang, *J. Eng. Manuf.*, 229 (2015) 421.
11. J.C. Walker, T.J. Kamps, J. W. Lam, J. Mitchell-Smith and A.T. Clare, *Wear*, 376-377 (2017) 1611.
12. A. Speidel, J. Mitchell-Smith, D.A. Walsh, M. Hirsch and A. Clare, Electrolyte Jet Machining of Titanium Alloys using Novel Electrolyte Solutions, 18th CIRP Conference on Electro Physical and Chemical Machining, Tokyo, Japan, 2016, 367
13. C. Guo, J. Qian and D. Reynaerts, *Micromach.*, 8 (2017) 143.
14. M. Hackert-Oschätzchen, A. Martin, G. Meichsner, M. Zinecker and A. Schubert, *Precis. Eng.*, 37 (2013) 621.
15. J. Kozak and K.E. Oczoś, *J. Mater. Process. Technol*., 109 (2001) 360.
16. Z. Liu, H. Nouraei, J.K. Spelt and M. Papini, *Precis. Eng*., 40 (2015) 189.
17. Z. Liu, H. Nouraei, M. Papini and J.K. Spelt, *J. Mater. Process. Technol*., 214 (2014) 1886.
18. G. Zhou and S.C. Yao, *Appl. Therm. Eng*., 31 (2011) 228.
19. R.H.M. Jafar, J.K. Spelt and M. Papini, *Wear*, 303 (2013) 302.
20. J. Schwartzentruber, J.K. Spelt and M., *Int. J. Mach. Tools Manuf*., 122 (2017) 1.

21. S. Kouravand and B.M. Imani, *Mach. Sci. Technol*., 18 (2014) 299.
22. N.G. Patil and P.K. Brahmankar, Semi-empirical modeling of surface roughness in wire electro-discharge machining of ceramic particulate reinforced Al matrix composites, 18th CIRP Conference on Electro Physical and Chemical Machining, Tokyo, Japan, 2016, 280
23. M.J. Jackson and J.P. Davim, Machining with abrasives, Springer, (2011) London, U.K.
24. W. Natsu, T. Ikeda and M. Kunieda, *Precis. Eng*., 31 (2007) 33.
25. B. Jones, E.D. Schoen and D.C. Montgomery, *Qual. Eng.*, 28 (2016) 369.
26. M. Hackert-Oschätzchen, G. Meichsner, M. Zinecker, A. Martin and A. Schubert, *Precis. Eng.*, 36 (2012) 612.
27. J. Kozak, K.P. Rajurkar and R. Balkrishna, *J. Manuf. Sci. Eng.*, 118 (1996) 490.
28. M. Hackert-Oschätzchen, R. Paul, A. Martin, G. Meichsner, N. Lehnert and A. Schubert, *J. Mater. Process. Technol.*, 223 (2015) 240.
29. K. L. Pang, T. Nguyen, J. Fan and J. Wang, *Mach. Sci. Technol.*, 16 (2012) 547.
30. Z. Liu, C. Gao, K. Zhao and K. Wang, *Int. J. Adv. Manuf. Technol*., 95 (2018) 1143.